Ecotoxicology and Environmental Safety 241 (2022) 113728

Contents lists available at ScienceDirect

Ecotoxicology and Environmental Safety

journal homepage: www.elsevier.com/locate/ecoenv

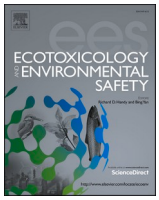

SETApp: A machine learning and image analysis based application to automate the sea urchin embryo test

Iker Alvarez-Mora [a,b,*,1], Leire Mijangos [a,b,2], Naroa Lopez-Herguedas [a,b,3], Jose M. Amigo [a,d,4], Harkaitz Eguiraun [b,c,5], Maddi Salvoch [a,b], Mathilde Monperrus [e,6], Nestor Etxebarria [a,b,7]

[a] Department of Analytical Chemistry, University of the Basque Country, Leioa, Biscay, Basque Country 48080, Spain
[b] Plentzia Marine Station, University of the Basque Country, Plentzia, Biscay, Basque Country 48620, Spain
[c] Department of Graphic Design and Engineering Projects, University of the Basque Country, Bilbao, Biscay, Basque Country 48013, Spain
[d] Ikerbasque, Basque Foundation for Science, Bilbao, Biscay, Basque Country 48009, Spain
[e] Institut des Sciences Analytiques et de Physico-chimie pour l'Environnement et les matériaux, Université de Pau et des Pays de l'Adour, Angelu, Basque Country 64000, France

ARTICLE INFO

Edited by Hao Zhu

Keywords:
Sea urchin embryo test
High-throughput screening
Machine learning
Image analysis
Ecotoxicology
Effect-directed analysis

ABSTRACT

Since countless xenobiotic compounds are being found in the environment, ecotoxicology faces an astounding challenge in identifying toxicants. The combination of high-throughput in vivo/in vitro bioassays with high-resolution chemical analysis is an effective way to elucidate the cause-effect relationship. However, these combined strategies imply an enormous workload that can hinder their implementation in routine analysis. The purpose of this study was to develop a new high throughput screening method that could be used as a predictive expert system that automatically quantifies the size increase and malformation of the larvae and, thus, eases the application of the sea urchin embryo test in complex toxicant identification pipelines such as effect-directed analysis. For this task, a training set of 242 images was used to calibrate the size-increase and malformation level of the larvae. Two classification models based on partial least squares discriminant analysis (PLS-DA) were built and compared. Moreover, Hierarchical PLS-DA shows a high proficiency in classifying the larvae, achieving a prediction accuracy of 84 % in validation. The scripts built along the work were compiled in a user-friendly standalone app (SETApp) freely accessible at https://github.com/UPV-EHU-IBeA/SETApp. The SETApp was tested in a real case scenario to fulfill the tedious requirements of a WWTP effect-directed analysis.

1. Introduction

Efforts to better understand the chemical and ecotoxicological characterization of the wastes released into the environment have addressed a set of organic micropollutants as contaminants of emerging concern (CECs) (Pontius, 2021; Tang et al., 2020). Some studies pointed out that wastewater treatment plants (WWTPs) can barely remove them from wastewater, making WWTP effluents a complex mixture of compounds with a high range of ecotoxicological effects (Loos et al., 2013; McCance et al., 2018; Mijangos et al., 2018). The ecotoxicological and analytical challenges lie in the complexity of these mixtures and the relationships between the presence of certain compounds and the toxicological endpoints (Krewski et al., 2010). Although many bioassays, both in vitro and in vivo, are commonly used for risk assessment, they do

* Correspondence to: Department of Analytical Chemistry, Faculty of Science and Technology, Bilbao, Basque Country 48080, Spain.
E-mail addresses: iker.alvarez@ehu.eus (I. Alvarez-Mora), leire.mijangos@ehu.eus (L. Mijangos), Naroa.lopez@ehu.eus (N. Lopez-Herguedas), josemanuel.amigo@ehu.eus (J.M. Amigo), Harkaitz.eguiraun@ehu.eus (H. Eguiraun), msalvoch001@ikasle.ehu.eus (M. Salvoch), mathilde.monperrus@univ-pau.fr (M. Monperrus), Nestor.etxebarria@ehu.eus (N. Etxebarria).
[1] ORCiD: 0000-0002-9814-2079.
[2] ORCiD: 0000-0003-1872-4624.
[3] ORCiD: 0000-0002-6501-2024.
[4] ORCiD: 0000-0003-1319-1312.
[5] ORCiD: 0000-0002-4014-6376.
[6] ORCiD: 0000-0002-6337-1672.
[7] ORCiD: 0000-0002-2942-9463.

https://doi.org/10.1016/j.ecoenv.2022.113728
Received 9 March 2022; Received in revised form 24 May 2022; Accepted 30 May 2022
Available online 8 June 2022
0147-6513/© 2022 The Author(s). Published by Elsevier Inc. This is an open access article under the CC BY license (http://creativecommons.org/licenses/by/4.0/).

not provide further information about the cause of the effects observed. Thus, in vivo bioassays are often coupled to chemical analysis techniques to explain these cause-effect relationships.

Effect-directed analysis (EDA) and toxicity identification evaluation (TIE) are the best available strategies for toxicant identification approaches (Brack et al., 2016; Burgess et al., 2013). Whichever the approach is, these strategies eventually require a long study to elucidate the cause-effect relation. In this regard, implementing high-throughput screening (HTS) methods is crucial to deal with this elucidation (Villeneuve et al., 2019) since many HTS platforms have taken a big step towards deploying complex and laborious methodologies in routine analysis through in vitro (Arini et al., 2017; Wetmore et al., 2015) and in vivo (Letamendia et al., 2012) bioassays.

The sea urchin (*Paracentrotus lividus*) embryo test (SET) has arisen as a key in vivo assay for coastal marine ecosystems. Apart from being affordable for use and maintenance, many studies have proven their sensitivity to emerging contaminants (Gambardella et al., 2016; Vethaak et al., 2017) and the suitability of this bioassay in EDA strategies (Mijangos et al., 2020). The two endpoints of this bioassay, the size increase, and the malformation level, are typically assessed by optical microscope observation. In the former case, the size increase from the egg to the 48 h larvae is compared. In addition to this, the reference criteria for malformation classification differentiate four malformation levels including, normal development (level 0), incorrect location of skeletal rods (level 1), incomplete or absence of skeletal rods (level 2), and blocked development (level 3) (Carballeira et al., 2012). Since implementing SET on a routine basis to tackle high-throughput analysis demands a large number of assays, image analysis, and machine learning techniques may find their way towards the automation of this bioassay (Nyffeler et al., 2020; Ramakumar et al., 2015).

The use of high-resolution digital microscope images combined with chemometric tools provides fast procedures to address high-throughput analysis, as recently shown in food control (Tormena et al., 2021) or microplastic analysis (da Silva et al., 2020) and more affordable than those based on deep learning microscopy (von Chamier et al., 2021). Within these tools, partial least squares discriminant analysis (PLS-DA) models are widely spread as they combine dimensionality reduction and discriminant analysis for predictive and descriptive modeling (Brereton, 2000). The method builds a linear model and classification boundaries that can be used as image classifiers (McEvoy and Amigo, 2013). Thus, the model requires a training set containing enough information to optimize the algorithm parameters to establish these boundaries. Validation of the built classifier is the most important step in any machine learning application; therefore, a test set must be used to construct the model (and calculate the boundaries); and a validation set must be used to test the performance of the previously created model.

This study aimed to develop an image analysis and machine learning-based pipeline to automate the SET. The proposed methodology would replace the traditional microscopic inspection of the larvae, providing comparable and observer-independent results reducing the workload and times in a user-friendly format. For a given image set of larvae exposed to any sample, the developed tool would give quantitative results for the two SET endpoints and build dose-response curves according to the concentration that the user introduces. In addition, to show the outputs obtained from this novel HTS method and prove its benefits, the developed app was implemented in the effect-directed analysis of Bayonne's WWTP effluent.

2. Experimental section

2.1. Sea urchin embryo test

Adult sea urchins were collected from the intertidal area of Armintza (43.43347°N, 2.89889°W, Basque Country) and maintained in aquaria at the Plentzia Marine Station (PiE). The temperature of the water was kept at 15 ± 1 °C, and the room was programmed with a natural photoperiod. Gametes and embryos were obtained following the procedure described by Mijangos et al. (Mijangos et al., 2020).

Fertilized sea urchin eggs were exposed for 48 h to four compounds independently and in five different concentrations (1 $\mu g \cdot L^{-1}$ - 5 $\mu g \cdot L^{-1}$ - 50 $\mu g \cdot L^{-1}$ - 500 $\mu g \cdot L^{-1}$ and 5 $mg \cdot L^{-1}$, 2 mL, n = 2) in 20 mL glass vials with 100 $egg \cdot mL^{-1}$ density. The selected compounds were albendazole, amitriptyline, copper (II) chloride and caffeine (Sigma Aldrich; St. Louis, MO, USA). In previous works, albendazole and amitriptyline were pointed out as important contributors to the toxicity of a WWTP effluent in EDA using the SET. Copper (II) chloride is a reagent typically used as a positive control in the SET methodology, and the morphological changes that this compound causes to sea urchin larvae have been deeply studied (Saco-Álvarez et al., 2010). Finally, caffeine was chosen for its mode of action (central-nervous-system stimulator), which differs from the aforementioned compounds. At 48hpf, larvae were fixed with formalin and transferred to 24-well-microplates. Each microplate row corresponded to six replicates of 200 μL.

2.2. Image acquisition and processing

Training and test image sets for the classification model construction were created using bright field pictures of sea-urchin larvae at 48 h post-fertilization (hpf). Images of non-exposed control embryos were also taken. Cytation™ 5 (4x magnification objective, BIOTEK) image reader was used to automatically obtain an image mapping of 25 pictures per well all over the plates. The imaging conditions suggested for an optimal larva separation using Cytation5 are LED intensity = 2; IT = 115; CG = 4 and Focus Height = 2750 μm. The imaging conditions were optimized using GEN5 software (BIOTEK) to ensure an appropriate focus and contrast of the larvae. Raw images were saved as *Tagged Image File Format* (.tif).

The images were processed to obtain a collection of up to 272 orientated and normalized larva pictures (Fig. 1) using homemade scripts in MATLAB® (Mathworks®, R2019b) supported by the Image Processing Toolbox™. The larvae image collection was classified by experts into three groups according to their degree of alteration as proposed by Carballeira et al. (Carballeira et al., 2012), but combining the two intermediate states (levels 1 and 2). The image set was randomly split into two groups: a training set (~90 %) consisting of 242 larva images to train the model and a test set of 30 images (~10 %) to estimate the performance of the measurements. The training set was revised to embrace all kinds of malformations (i.e., all the phenotypes described by Carballeira et. al. (Carballeira et al., 2012): crossed tip, separated tip fused arms, incomplete or absent skeletal rods, absence of skeletal rods, and folded tip, fractured ectoderm, undeveloped embryos). This way, the model was not biased towards any particular phenotype, and every larva was considered independent regardless of the experiment they came.

The image of each larva was parametrized, calculating N = 14 image parameters concerning the shape of the larva (Table 1). Following this strategy, each larva was encoded to be the m^{th} row of a matrix $\mathbf{X}$ (M x N), where the values of each parameter were placed in the N columns. The PLS-DA models were built using the Classification Toolbox built by Ballabio and Consonni (Ballabio and Consonni, 2013) working under a Matlab environment using randomized subset cross-validation to assure the independence of the validation subsets. The external validation was carried out by predicting the malformation level of the larvae belonging to the test set and comparing them to the level determined by the experts. The sensitivity (estimation of the model ability to avoid false negatives), specificity (estimation of the model ability to avoid false positives), and the prediction error were calculated as outlined by Ballabio et al. (Ballabio et al., 2018).

An additional experiment to validate the size increase measurement was carried out by exposing the larvae to copper (II) chloride. The approach described by Carballeira et al. was implemented by two experts measuring the larvae under an inverted microscope coupled to an

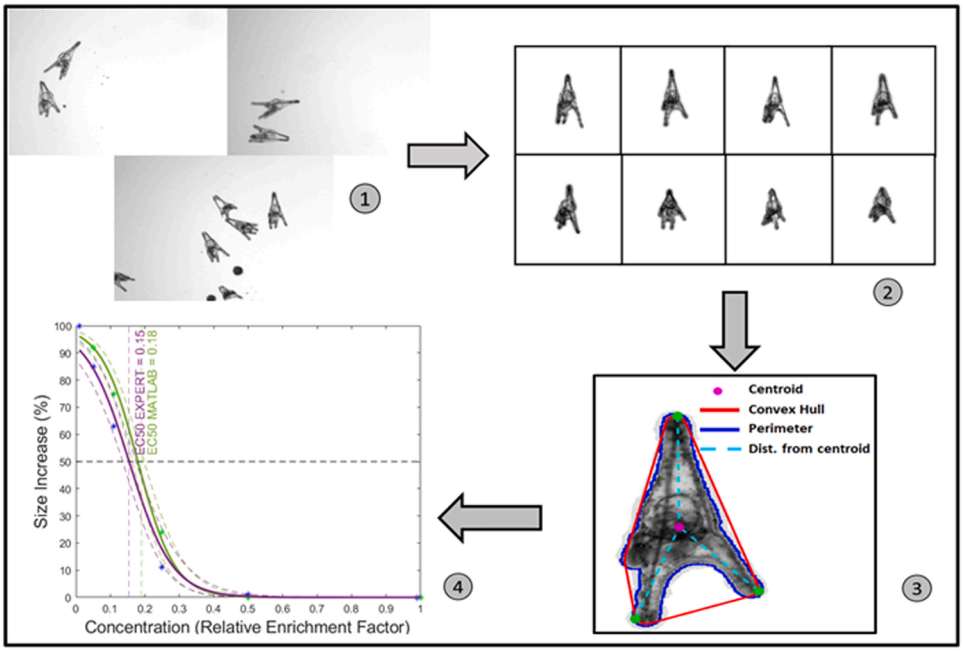

Fig. 1. Flow chart of the image processing. (1) Raw images. (2) Processed images. (3) Image parametrization. (4) Dose-response curves built from image parameters.

Table 1
Parameters used in the classification model to predict the malformation level.

Parameter	Definition
Alpha	Angle between the centroid-left leg and centroid-right leg vectors
Area	Area of the extracted larva image
Area Ratio	Ratio between the extracted larva image area and the convex hull associated with that image
Beta	Angle between the top-left leg and top-right leg vectors
Circularity	Circularity of the extracted larva image
Convex Hull Area	Area of the convex hull associated with the extracted larva image
Left Leg Distance	Euclidean distance between the centroid and the left leg
Leg Size Ratio	Ratio between Left Leg Distance and Right Leg Distance
Mayor Axis Length	Euclidean distance of the extracted mayor axis of the larva
Minor Axis Length	Euclidean distance of the extracted minor axis of the larva
Perimeter	Perimeter of the extracted larva image
Right Leg Distance	Euclidean distance between the centroid and the right leg
Size	Euclidean distance from the top to the furthest point of the leg
TopSum	Number of pixels within the first ten image rows (gives information about the top shape of the larva)

electronic camera and using NIS-Elements image analysis software v4.30 (Nikon Instruments BV, Europe). Three larvae groups exposed to different concentrations of $CuCl_2$ were measured and compared to the size measurements obtained in the parametrization.

The MATLAB App Designer was used to compile the image processing, analysis, and modelling scripts in a standalone app. The classification models built in the Classification Toolbox were also compiled within the app and used to predict a new outcome from the image sets that the user loads. The logit function was implemented for dose-response curves to fit the quantified endpoints to the concentration data that the user can introduce.

2.3. Implementation of the SETApp on effect-directed analysis

To test the performance of the SETApp in a real and demanding scenario, we implemented it in the effect-directed analysis of Bayonne's (France) Pont de l'aveugle WWTP effluent to assess the impact of this effluent in the Adour estuary. The benefits of using this new approach over the traditional strategy were studied, and both methodologies were compared.

An automatic large volume solid-phase extraction system (LV-SPE, MAXX Mess-u. Probenahmetechnik GmbH, Rangendingen, Germany) was used to sample 17 L of Bayonne's (France) Pont de l'aveugle WWTP effluent. Reverse-phase, cationic exchanger, and anionic exchanger-based in-house cartridges (6 g Strata HR-X, 2 g Strata ZT-WAX, and 2 g Strata ZT-WCX) were used for analyte extraction. The extracts were pooled and evaporated in a rotary evaporator (LABOROTA 4000, Heidolph Laborota 4000, Schwabach, Germany, and Büchi B-480 water bath, Flawil, Switzerland) to 15 mL obtaining a relative enrichment factor (REF) of 1133.

The raw sample was then subjected to a fractioning step using semi-preparative reverse-phase liquid chromatography (C_{18} column, 250 ×10 mm, 5 μm particle size, Phenomenex Gemini®, CA, USA) coupled to an automatic fraction collector (Agilent 1260 Infinity II, Santa Clara, CA, USA) under the control of ChemStation C.01.08 software. The fractioning conditions described by Mijangos et al. (Mijangos et al., 2020) were followed to obtain 17 fractions, and SET was applied to fractions 3–17 (no compounds were expected in samples 1 and 2 due to the dead volume of the system). Suspect screening using UHPLC-HRMS was restricted to toxic fractions, and raw and recombined samples. The conditions of the chemical analysis and the suspect screening workflow (Fig. S2) are described in the Supporting information (SI.2 and SI.3).

For fractions 3–17, larvae (100 eggs/mL, 2 mL, n = 2) were exposed for 48 h to each sample at REF 30 (H_2O, 0.1 % DMSO) in 10 mL vials. After 48 h, larvae were fixed with formalin, transferred to 24-well microplates, and the images were read and processed using the SETApp. Four control groups were also prepared in H_2O, 0.1 % DMSO. Two were fixed at t = 0 h and used as the egg control group; two were fixed at t = 48 h and used as the developed control group. In total, 17 microplates were submitted for image acquisition. Dose-response curves were built for fractions showing toxicity at REF 30, and EC_{50} values were calculated.

3. Results and discussions

3.1. SET automation

Image binarization based on pixel intensity was applied to extract the individual pictures of the larvae from the raw image containing an undefined number of larvae. The binary image was submitted to a dilation, removing small artifacts and elements in the borders of the picture. This processed binary image was used to localize individual larvae and extract, rotate and normalize each larva from the original image. The individual larvae pictures are then saved in 500 × 400, *.tiff* format. The full workflow is described within the Supporting information (SI.1).

A set of 242 larvae pictures covering a wide range of different degrees of physical alteration was obtained to build the training set and 30 extra images as the test set. The expert panel classified 37 larvae as level 0, 107 as level 1 (corresponding to levels 1 and 2 of Carballeira et al. (Carballeira et al., 2012)), and 98 as level 2. The image parameters chosen to explain the differences between alteration levels are summarized in Table 1 and used as input for the two PLS-DA models tested. Whereas the first model gave optimal results with 4 latent variables (59 %, 11 %, 9 %, and 5 % of the total explained variance), 3 latent variables were selected in each of the sequential models of the HPLS-DA (51 %, 8 % and 9 % of the total explained variance for the first model and 32 %,10 % and 10 % for the second). The scores and loadings scatter plots of latent variable 1 against latent variable 2 are displayed in Fig. 3. Different groups can be observed in the scores scatter plot (Fig. 2). These results were compared to those obtained by a Hierarchical PLS-DA (HPLS-DA) built by two consecutive PLS-DA and, thus, having 2 stages. The first stage separates levels 0 and 1 from level 2, and the second one separates levels 0 from 1.

3.2. Validation of the classification model

Both approaches were built and validated with the same training and test sets, and their performance was compared. Overall performance figures of the two approaches are shown in Table 2, while for the selected model, the classification performance for each of the three levels and the confusion matrix is deeper explained in Table SI.4. In general, more accurate performance in sensitivity (84 %), specificity (95 %) and prediction error can be observed in the Hierarchical PLS-DA. The total classification uncertainty (15.6 %) was in agreement with the one expected from the panel of experts. We have demonstrated that a concise and comprehensive parametrization of the samples, followed by a linear classification method gives accurate results.

Table 2
Comparison between the studied classification performance of the model.

	HPLS-DA		PLS-DA	
	TRAINING	TEST	TRAINING	TEST
Sensitivity	0.916	0.844	0.908	0.806
Specificity	0.954	0.952	0.920	0.902
Prediction error	0.084	0.156	0.092	0.194

3.3. Validation of the size-increase measurement

In order to validate our approach, a new experiment was run. The length of three exposed ($CuCl_2$ 0.01, 0.1, 0.5 mg·L^{-1}) embryo groups and an egg control group was measured in parallel by two experts under the microscope and the automatized pipeline. The comparative results are displayed in SI.5. In order to compare the size increase between groups, the mean length of the eggs was subtracted from each experimental measure (e.g. 1st expert Eggs subtracted to $CuCl_2$ 0.01 mg·L^{-1}). We observed that the difference between groups increases as the size of the larvae decreases. Still, comparable results were obtained (for $CuCl_2$ 0.01, 0.1 & 0.5 mg·L^{-1}; ρ-level > 0.05) between the three methods at all the concentration levels.

Furthermore, dose-response curves of a contaminated water sample were built simultaneously using manual measurements from expert and

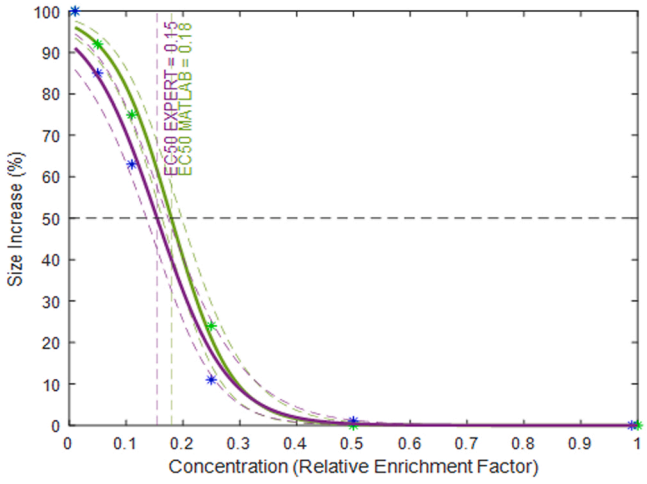

Fig. 3. Dose-response curves of the same sample, built by Sea Urchin App (green) and an expert (purple).

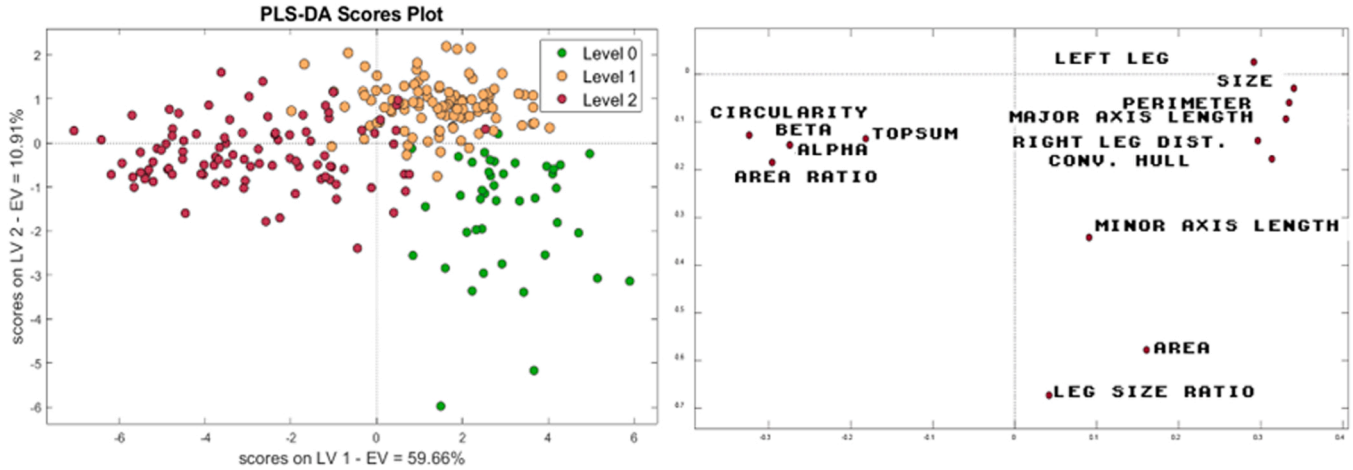

Fig. 2. Scores and Loadings plots of the PLS-DA model built with three classes. Each color corresponds to a malformation level.

automatized measurements (Fig. 3), and comparable results were obtained within a 95 % confidence level.

3.4. SETApp (v1.0)

Considering the obtained results, HPLS-DA was chosen to implement a MATLAB-based Application (SETApp) in the automatized sea urchin embryo test pipeline. This way, a standalone app (SETApp) has been released and is freely accessible at https://github.com/UPV-EHU-IBeA/SETApp. Overall, the SETApp allows the user to measure and classify every sea-urchin larvae in a given digital microscope image and export the results and dose-response curves. The simplified graphical interface enables the user to select the path to folders, process, measure, and classify the images in a very intuitive manner.

The SETApp includes two tabs, the Measurement, and the Classification tabs. The Measurement tab contains three folder browser buttons, egg group image selection (needed for growth calculation), control group selection, and sample selection (see SI.1). Thus, the only input that SETApp requires is the path to the image folders. Worth mentioning that the possibility to have subfolders inside the sample folder was also considered so every subfolder would be analyzed as parallel sample groups. A tutorial on the app's functioning with interface pictures can be found in Supporting information.

The process button starts the image processing of the images within the selected folders. No output is shown in the app after processing, but new images with the extracted larvae will automatically appear in each folder. The user can check these images in search of any artifact that could have been mistaken for actual larvae and remove it. Measure button reads the extracted larvae and measures them. The results are displayed in a bar plot and a table including the mean length ($\bar{l}$) of the larvae in each folder, the standard deviation, and the size increase (SI) percentage, calculated with the following equation:

$$SI(\%) = \frac{\bar{l}_{sample} - \bar{l}_{egg}}{\bar{l}_{control} - \bar{l}_{egg}} \times 100 \quad (1)$$

If necessary, the Measure Tab also includes a dose-response curve building option. The exposure concentrations can be introduced in the boxes included. Since the most common curve fitting algorithms in dose-response relationships are logistic regression analysis (logit) and probit analysis, logit has been implemented in the app, and dose-response curve charts can be visualized by pressing the *Build Curve* button.

On the other hand, the Classification Tab uses the already processed images to parametrize them and predict the malformation level of each larva using the chosen HPLS-DA model. In this case, the index of toxicity (IT) equation has been slightly modified from Carballeira et al. (Carballeira et al., 2012) to:

$$IT = \frac{0 \times \%level_0 + 1.5 \times \%level_1 + 3 \times \%level_2}{100} \quad (2)$$

The unification of levels 1 and 2 into new level 1 forces us to adapt the middle weight to 1.5, outlining the agreement between both methodologies. The combination of levels 1 and 2 could result in a loss of information for interpretation purposes. Thus, the processed images are saved in the folders and can be checked for further studies. IT results are displayed in a bar plot and a table, and they can also be used to build a dose-response curve.

Shortly, when the dataset is large enough, we will address the implementation of a new version based on deep convolutional architecture to improve the classification performance. Improvements in the classification model would bring the distinction between levels 1 and 2, and, at best, the classification between phenotypes, which would offer valuable information about the mode of action of the contaminants.

3.5. Implementation of the SETApp on effect-directed analysis of Bayonne's WWTP effluent

After the fractionation of the sample, images of the microplates with exposed larvae, developed controls, and egg controls were obtained. The results acquired from the SETApp after loading, processing, and measuring the images showed that fractions F4, F5, F7, F10, and F12 exhibited embryo growth inhibition at REF 20 (SI < 80 %) (Fig. 4. A). When category 2 bioassays (i.e., non-specific bioassays indicative of adaptive stress responses or apical endpoints) such as the SET are applied, the distribution of the bioactivity over multiple fractions is typically spread (Escher et al., 2021), as was observed in these results. For further prioritization between toxic fractions, REF 30 was also tested (Fig. 4. B). The bioassay carried out at REF 30 pointed out F10 and F4 as the main concerning fractions.

Dose-response curves of F4 and F10 were built in the SETApp (Fig. 5). F10 showed significantly higher toxicity ($EC_{50,F10}$ = 9.30; $EC_{50,F4}$ = 38) than F4. Therefore, toxicant identification efforts were focused on F10, and suspect screening was restricted to this fraction.

The implementation of the SETApp reduced the time to assess the toxicity from days to hours, and we can conclude that the developed application can be used as an efficient, fast, cost-effective, and reproducible tool to emulate the SET that fits remarkably well in EDA.

F10, raw eta recombined samples were analyzed to identify the most likely toxic candidates following the workflow described in Section 1 of the Supporting information. The preliminary output from this analysis rendered more than 2500 features. The list of candidates was drastically reduced to < 70 after applying a set of postrun filters. Among them, 4 were identified (Level 1) and 2 tentatively identified as probable structures (Level 2a) according to the classification by Schymanski et al. (Schymanski et al., 2014) (Table 3).

4. Conclusions

In conclusion, we have developed a novel predictive expert system, the SETApp, that can be used to automatically quantify the two endpoints of the sea urchin embryo test from a given image set. We have demonstrated that chemometrics, and specially multivariate linear classification models, can be successfully implemented in bioassay automation to avoid the cumbersome measurement of the embryo sizes and malformation levels. Furthermore, the SETApp provides the numerical estimation of the endpoints, including the dose-effect curve fitting and the estimation of the ECx values, if required. In addition, we have shown the efficiency of this HTS in a very demanding scenario, the EDA of Bayonne's (France) Pont de l'aveugle WWTP effluent. This EDA study concluded that the SETApp is an efficient, fast, cost-effective, and reproducible tool that can approach EDA to routine analysis.

CRediT authorship contribution statement

Iker Alvarez-Mora (I.Alvarez-Mora) – Conceptualization, Methodology, Software, Validation, Investigation, Writing – original draft, Writing – review & editing, Visualization. Jose Manuel Amigo (Jose M. Amigo) – Conceptualization, Software, Validation, Writing – review & editing, Visualization, Supervision. Leire Mijangos (Leire Mijangos) – Conceptualization, Methodology, Writing – review & editing, Investigation. Naroa Lopez-Herguedas (N. Lopez-Herguedas) – Conceptualization, Methodology, Investigation, Writing – review & editing. Harkaitz Eguiraun (H. Eguiraun) – Conceptualization. Mathilde Monperrus (M.Monperrus) – Resources, Project administration. Maddi Salvoch (M. Salvoch) – Investigation. Nestor Etxebarria (N. Etxebarria) – Conceptualization, Methodology, Investigation, Resources, Writing – original draft, Writing – review & editing, Supervision, Project administration, Funding acquisition.

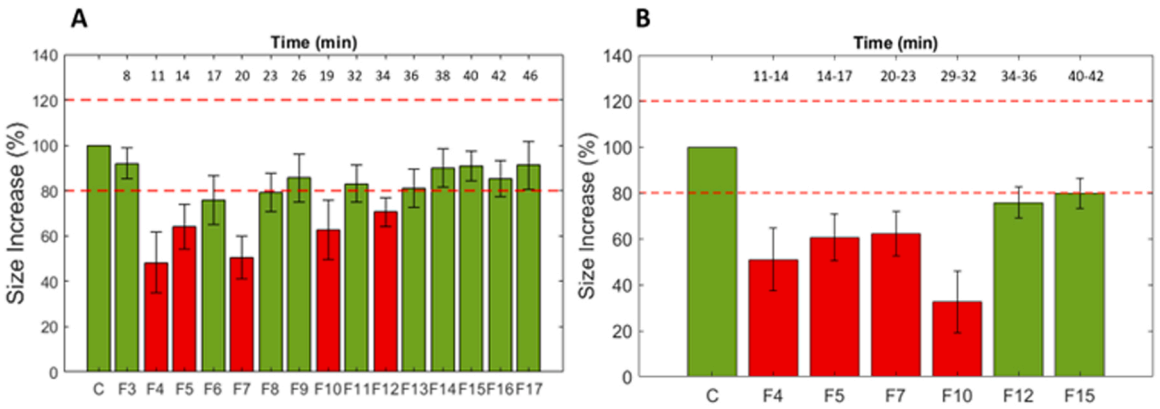

Fig. 4. Response in SET of all the fractions at REF 20 (A) and toxic fractions at REF 30 (B). Red bars refer to toxic fractions. F15 was included at REF 30 as the negative control of the samples.

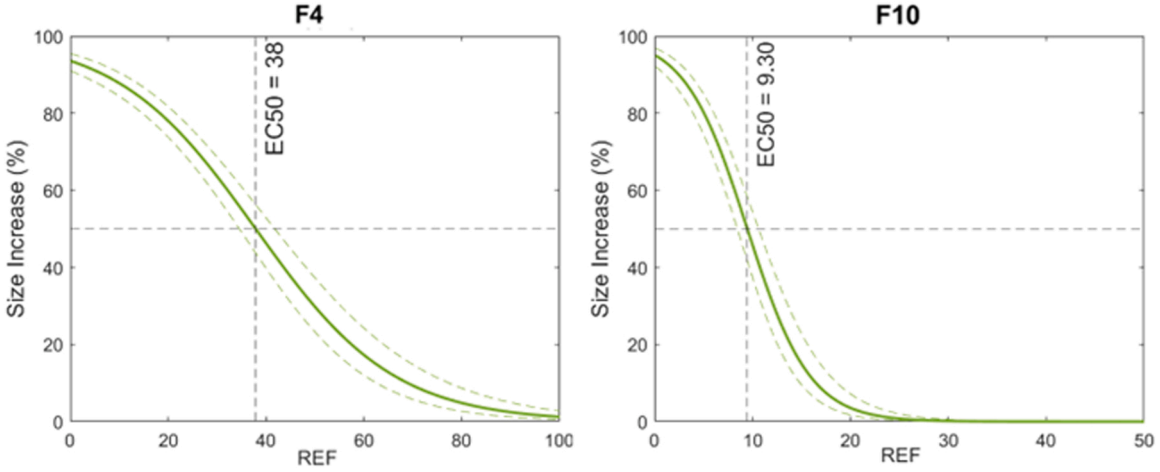

Fig. 5. Dose-response curve of the toxic fractions (F4 and F10), including EC_{50} values.

Table 3
Overview of the seven identified features in F10.

COMPOUND	FORMULA	ESI MODE	*m/z*	t_R (min)	mzCloud Match	Level
Carbamazepine	$C_{15}H_{12}N_2O$	[M+H]	236.09496	7.80	99	1
Cetirizine	$C_{21}H_{27}Cl_3N_2O_3$	[M+H]	388.15537	7.40	89.1	1
Terbutryn	$C_{10}H_{19}N_5S$	[M+H]	241.13611	8.70	97.7	1
2-Hydroxybenzothiazole	C_7H_5NOS	[M+H]	151.00918	5.70	93.7	1
4-Methylbenzotriazole	$C_7H_7N_3$	[M+H]	133.06387	4.49	98.3	2a
Terbumeton	$C_{10}H_{19}N_5O$	[M+H]	225.1587	5.73	71.4	2a

Declaration of Competing Interest

The authors declare that they have no known competing financial interests or personal relationships that could have appeared to influence the work reported in this paper.

Acknowledgements

Authors gratefully acknowledge financial support from the Agencia Estatal de Investigación (AEI) of Spain and the European Regional Development Fund through project CTM2017–84763-C3–1-R and the Basque Government through the financial support as a consolidated group of the Basque Research System (IT1213–19). Iker Alvarez is grateful to the University of the Basque Country and the Université de Pau et des Pays de L′ Adour for his cotutelle predoctoral scholarship.

Appendix A. Supporting information

Supplementary data associated with this article can be found in the online version at doi:10.1016/j.ecoenv.2022.113728.

References

Arini, A., Mittal, K., Dornbos, P., Head, J., Rutkiewicz, J., Basu, N., 2017. A cell-free testing platform to screen chemicals of potential neurotoxic concern across twenty vertebrate species. Environ. Toxicol. Chem. 36, 3081–3090. https://doi.org/10.1002/etc.3880.

Ballabio, D., Consonni, V., 2013. Classification tools in chemistry. Part 1: linear models. PLS-DA. Anal. Methods 5, 3790–3798. https://doi.org/10.1039/C3AY40582F.

Ballabio, D., Grisoni, F., Todeschini, R., 2018. Multivariate comparison of classification performance measures. Chemom. Intell. Lab. Syst. 174, 33–44. https://doi.org/10.1016/j.chemolab.2017.12.004.

Brack, W., Ait-Aissa, S., Burgess, R.M., Busch, W., Creusot, N., Di Paolo, C., Escher, B.I., Mark Hewitt, L., Hilscherova, K., Hollender, J., Hollert, H., Jonker, W., Kool, J., Lamoree, M., Muschket, M., Neumann, S., Rostkowski, P., Ruttkies, C., Schollee, J.,

Schymanski, E.L., Schulze, T., Seiler, T.-B., Tindall, A.J., De Aragão Umbuzeiro, G., Vrana, B., Krauss, M., 2016. Effect-directed analysis supporting monitoring of aquatic environments–an in-depth overview. Sci. Total Environ. 544, 1073–1118. https://doi.org/10.1016/j.scitotenv.2015.11.102.

Brereton, R.G., 2000. Introduction to multivariate calibration in analyticalchemistry. Analyst 125, 2125–2154. https://doi.org/10.1039/B003805I.

Burgess, R.M., Ho, K.T., Brack, W., Lamoree, M., 2013. Effects-directed analysis (EDA) and toxicity identification evaluation (TIE): complementary but different approaches for diagnosing causes of environmental toxicity. Environ. Toxicol. Chem. 32, 1935–1945. https://doi.org/10.1002/etc.2299.

Carballeira, C., Ramos-Gómez, J., Martín-Díaz, L., DelValls, T.A., 2012. Identification of specific malformations of sea urchin larvae for toxicity assessment: application to marine pisciculture effluents. Mar. Environ. Res. 77, 12–22. https://doi.org/10.1016/j.marenvres.2012.01.001.

von Chamier, L., Laine, R.F., Jukkala, J., Spahn, C., Krentzel, D., Nehme, E., Lerche, M., Hernández-Pérez, S., Mattila, P.K., Karinou, E., Holden, S., Solak, A.C., Krull, A., Buchholz, T.-O., Jones, M.L., Royer, L.A., Leterrier, C., Shechtman, Y., Jug, F., Heilemann, M., Jacquemet, G., Henriques, R., 2021. Democratising deep learning for microscopy with ZeroCostDL4Mic. Nat. Commun. 12, 2276. https://doi.org/10.1038/s41467-021-22518-0.

da Silva, V.H., Murphy, F., Amigo, J.M., Stedmon, C., Strand, J., 2020. Classification and quantification of microplastics (<100 μm) using a focal plane Array–Fourier transform infrared imaging system and machine learning. Anal. Chem. 92, 13724–13733. https://doi.org/10.1021/acs.analchem.0c01324.

Escher, B., Neale, P., Leusch, F., 2021. Bioanalytical Tools in Water Quality Assessment. ⟨https://doi.org/10.2166/9781789061987⟩.

Gambardella, C., Ferrando, S., Gatti, A.M., Cataldi, E., Ramoino, P., Aluigi, M.G., Faimali, M., Diaspro, A., Falugi, C., 2016. Review: morphofunctional and biochemical markers of stress in sea urchin life stages exposed to engineered nanoparticles. Environ. Toxicol. 31, 1552–1562. https://doi.org/10.1002/tox.22159.

Krewski, D., Acosta, D., Andersen, M., Anderson, H., Bailar, J.C., Boekelheide, K., Brent, R., Charnley, G., Cheung, V.G., Green, S., Kelsey, K.T., Kerkvliet, N.I., Li, A.A., McCray, L., Meyer, O., Patterson, R.D., Pennie, W., Scala, R.A., Solomon, G.M., Stephens, M., Yager, J., Zeise, L., Staff of Committee on Toxicity Testing and Assessment of Environmental Agents, 2010. Toxicity testing in the 21st century: a vision and a strategy. J. Toxicol. Environ. Health Part B 13, 51–138. https://doi.org/10.1080/10937404.2010.483176.

Letamendia, A., Quevedo, C., Ibarbia, I., Virto, J.M., Holgado, O., Diez, M., Izpisua Belmonte, J.C., Callol-Massot, C., 2012. Development and validation of an automated high-throughput system for zebrafish in vivo screenings. PLoS One 7, e36690. https://doi.org/10.1371/journal.pone.0036690.

Loos, R., Carvalho, R., António, D.C., Comero, S., Locoro, G., Tavazzi, S., Paracchini, B., Ghiani, M., Lettieri, T., Blaha, L., Jarosova, B., Voorspoels, S., Servaes, K., Haglund, P., Fick, J., Lindberg, R.H., Schwesig, D., Gawlik, B.M., 2013. EU-wide monitoring survey on emerging polar organic contaminants in wastewater treatment plant effluents. Water Res. 47, 6475–6487. https://doi.org/10.1016/j.watres.2013.08.024.

McCance, W., Jones, O.A.H., Edwards, M., Surapaneni, A., Chadalavada, S., Currell, M., 2018. Contaminants of Emerging Concern as novel groundwater tracers for delineating wastewater impacts in urban and peri-urban areas. Water Res. 146, 118–133. https://doi.org/10.1016/j.watres.2018.09.013.

McEvoy, F.J., Amigo, J.M., 2013. Using machine learning to classify image features from canine pelvic radiographs: evaluation of partial least squares discriminant analysis and artificial neural network models. Vet. Radio. Ultrasound 54, 122–126. https://doi.org/10.1111/vru.12003.

Mijangos, L., Ziarrusta, H., Ros, O., Kortazar, L., Fernández, L.A., Olivares, M., Zuloaga, O., Prieto, A., Etxebarria, N., 2018. Occurrence of emerging pollutants in estuaries of the Basque Country: analysis of sources and distribution, and assessment of the environmental risk. Water Res. 147, 152–163. https://doi.org/10.1016/j.watres.2018.09.033.

Mijangos, L., Krauss, M., de Miguel, L., Ziarrusta, H., Olivares, M., Zuloaga, O., Izagirre, U., Schulze, T., Brack, W., Prieto, A., Etxebarria, N., 2020. Application of the sea urchin embryo test in toxicity evaluation and effect-directed analysis of wastewater treatment plant effluents. Environ. Sci. Technol. 54, 8890–8899. https://doi.org/10.1021/acs.est.0c01504.

Nyffeler, J., Willis, C., Lougee, R., Richard, A., Paul-Friedman, K., Harrill, J.A., 2020. Bioactivity screening of environmental chemicals using imaging-based high-throughput phenotypic profiling. Toxicol. Appl. Pharmacol. 389, 114876 https://doi.org/10.1016/j.taap.2019.114876.

Pontius, F.W., 2021. Emerging contaminants in water: detection, treatment, and regulation. Water 13, 1470. https://doi.org/10.3390/w13111470.

Ramakumar, A., Subramanian, U., Prasanna, P.G.S., 2015. High-throughput sample processing and sample management; the functional evolution of classical cytogenetic assay towards automation. Mutation Research/Genetic Toxicology and Environmental Mutagenesis, Insights into formation and consequences of chromosome aberrations: Report on the 11th International Symposium on Chromosomal Aberrations (ISCA 11), Rhodes, Greece, September 12–14, 2014 793, 132–141. ⟨https://doi.org/10.1016/j.mrgentox.2015.07.011⟩.

Saco-Álvarez, L., Durán, I., Ignacio Lorenzo, J., Beiras, R., 2010. Methodological basis for the optimization of a marine sea-urchin embryo test (SET) for the ecological assessment of coastal water quality. Ecotoxicol. Environ. Saf. 73, 491–499. https://doi.org/10.1016/j.ecoenv.2010.01.018.

Schymanski, E.L., Jeon, J., Gulde, R., Fenner, K., Ruff, M., Singer, H.P., Hollender, J., 2014. Identifying small molecules via high resolution mass spectrometry: communicating confidence. Environ. Sci. Technol. 48, 2097–2098. https://doi.org/10.1021/es5002105.

Tang, Y., Zhong, Y., Li, H., Huang, Y., Guo, X., Yang, F., Wu, Y., 2020. Contaminants of emerging concern in aquatic environment: occurrence, monitoring, fate, and risk assessment. Water Environ. Res. 92, 1811–1817. https://doi.org/10.1002/wer.1438.

Tormena, C.D., Campos, R.C.S., Marcheafave, G.G., Edward Bruns, R., Scarminio, I.S., Pauli, E.D., 2021. Authentication of carioca common bean cultivars (Phaseolus vulgaris L.) using digital image processing and chemometric tools. Food Chem. 364, 130349 https://doi.org/10.1016/j.foodchem.2021.130349.

Vethaak, A.D., Hamers, T., Martínez-Gómez, C., Kamstra, J.H., de Weert, J., Leonards, P.E.G., Smedes, F., 2017. Toxicity profiling of marine surface sediments: a case study using rapid screening bioassays of exhaustive total extracts, elutriates and passive sampler extracts. Mar. Environ. Res. 124, 81–91. https://doi.org/10.1016/j.marenvres.2016.03.002. The ICON Project (the trans-European research project on field studies related to a large-scale sampling and monitoring.

Villeneuve, D.L., Coady, K., Escher, B.I., Mihaich, E., Murphy, C.A., Schlekat, T., Garcia-Reyero, N., 2019. High throughput screening and environmental risk assessment – state of the science and emerging applications. Environ. Toxicol. Chem. 38, 12–26. https://doi.org/10.1002/etc.4315.

Wetmore, B.A., Wambaugh, J.F., Allen, B., Ferguson, S.S., Sochaski, M.A., Setzer, R.W., Houck, K.A., Strope, C.L., Cantwell, K., Judson, R.S., LeCluyse, E., Clewell, H.J., Thomas, R.S., Andersen, M.E., 2015. Incorporating high-throughput exposure predictions with dosimetry-adjusted in vitro bioactivity to inform chemical toxicity testing. Toxicol. Sci. 148, 121–136. https://doi.org/10.1093/toxsci/kfv171.